4-26-2013

# Magnonlike Dispersion of Spin Resonance in Ni-doped BaFe2As2

M. G. Kim
*Iowa State University and Ames Laboratory*

G. S. Tucker
*Iowa State University and Ames Laboratory*

D. K. Pratt
*Iowa State University and Ames Laboratory*

S. Ran
*Iowa State University and Ames Laboratory*

A. Thaler
*Iowa State University and Ames Laboratory*

*See next page for additional authors*

# Magnonlike Dispersion of Spin Resonance in Ni-doped BaFe2As2


## Abstract

Inelastic neutron scattering measurements on Ba(Fe0.963Ni0.037)2As2 manifest a neutron spin resonance in the superconducting state with anisotropic dispersion within the Fe layer. Whereas the resonance is sharply peaked at the antiferromagnetic (AFM) wave vector QAFM along the orthorhombic a axis, the resonance disperses upwards away from QAFM along the b axis. In contrast to the downward dispersing resonance and hourglass shape of the spin excitations in superconducting cuprates, the resonance in electron-doped BaFe2As2 compounds possesses a magnonlike upwards dispersion.



## Disciplines

Condensed Matter Physics

## Comments

This article is published as Kim, M. G., G. S. Tucker, D. K. Pratt, S. Ran, A. Thaler, Andrew D. Christianson, K. Marty, S. Calder, A. Podlesnyak, S. L. Bud'ko, P. C. Canfield, A. Kreyssig, A. I. Goldman, and R. J. McQueeney. "Magnonlike Dispersion of Spin Resonance in Ni-doped Ba Fe 2 As 2." *Physical Review Letters* 110, no. 17 (2013): 177002. DOI: 10.1103/PhysRevLett.110.177002. Posted with permission.



## Authors

M. G. Kim, G. S. Tucker, D. K. Pratt, S. Ran, A. Thaler, A. D. Christianson, K. Marty, S. Calder, A. Podlesnyak, Sergey L. Bud'ko, Paul C. Canfield, Andreas Kreyssig, Alan I. Goldman, and Robert McQueeney

# Magnonlike Dispersion of Spin Resonance in Ni-doped $BaFe_2As_2$

M. G. Kim,[1,*] G. S. Tucker,[1] D. K. Pratt,[1] S. Ran,[1] A. Thaler,[1] A. D. Christianson,[2] K. Marty,[2] S. Calder,[2] A. Podlesnyak,[2] S. L. Bud'ko,[1] P. C. Canfield,[1] A. Kreyssig,[1] A. I. Goldman,[1] and R. J. McQueeney[1,†]

[1]*Ames Laboratory and Department of Physics and Astronomy, Iowa State University, Ames, Iowa 50011, USA*

[2]*Oak Ridge National Laboratory, Oak Ridge, Tennessee 37831, USA*

(Received 21 January 2013; published 24 April 2013)

Inelastic neutron scattering measurements on $Ba(Fe_{0.963}Ni_{0.037})_2As_2$ manifest a neutron spin resonance in the superconducting state with anisotropic dispersion within the Fe layer. Whereas the resonance is sharply peaked at the antiferromagnetic (AFM) wave vector $\mathbf{Q}_{\mathrm{AFM}}$ along the orthorhombic **a** axis, the resonance disperses upwards away from $\mathbf{Q}_{\mathrm{AFM}}$ along the **b** axis. In contrast to the downward dispersing resonance and hourglass shape of the spin excitations in superconducting cuprates, the resonance in electron-doped $BaFe_2As_2$ compounds possesses a magnonlike upwards dispersion.

DOI: 10.1103/PhysRevLett.110.177002 PACS numbers: 74.70.Xa, 74.20.Mn, 78.70.Nx

A spin resonance, observed in inelastic neutron scattering (INS) measurements, appears in superconducting (SC) materials that do not possess a simple *s*-wave gap symmetry [1,2]. Consequently, the spin resonance is considered to be a hallmark of unconventional superconductivity and highlights the important relationship between antiferromagnetic (AFM) spin fluctuations and superconductivity. The spin resonance has an intimate connection to the superconducting state [1–5]. The INS signature of the resonance is a gapping of normal state spin fluctuations at the AFM wave vector $\mathbf{Q}_{\mathrm{AFM}}$ for energies well below the superconducting gap $2\Delta$ and an enhancement of magnetic spectral weight at an energy $\Omega_0 < 2\Delta$. The energy of the resonance at $\mathbf{Q}_{\mathrm{AFM}}$ is found to be proportional to the SC transition temperature $T_c$ ($\Omega_0/k_BT_c \approx 4$–$6$) or $2\Delta$ ($\Omega_0/2\Delta \approx 0.6$) for a variety of unconventional superconductors [6,7]. The dispersion of the spin resonance $\Omega_{\mathbf{q}}$ (where $\mathbf{q} = \mathbf{Q} - \mathbf{Q}_{\mathrm{AFM}}$) is a measure of the resonance energy away from $\mathbf{Q}_{\mathrm{AFM}}$.

In the case of the single-band cuprates, the dispersion of spin fluctuations forms a characteristic hourglass shape below $T_c$ where the resonance appears at the neck of the hourglass with energy $\Omega_0$, as shown in Fig. 1(a) [3,4]. The downward dispersion ($\omega < \Omega_0$) is associated with the resonance itself $\Omega_{\mathbf{q}}$, whereas the upward dispersion ($\omega > \Omega_0$) arises from normal state spin waves [8]. In the cuprates, the downward resonance dispersion is determined by nodes in the *d*-wave SC gap at $\mathbf{q} = \mathbf{q}_{\mathrm{node}}$, where $\Delta_{\mathbf{q}_{\mathrm{node}}} = 0$.

Although the spin resonance has been clearly observed at $\mathbf{Q}_{\mathrm{AFM}}$ in multiband iron arsenide compounds studied to date, no dispersion of the resonance within the Fe layers (in the **ab** plane) has yet been reported and, complicating matters, band structure calculations predict both an upward [9] and a downward [10] dispersion depending on the details of the bands and the symmetry of the superconducting order parameter. In this Letter, we use inelastic neutron scattering to show that the resonance in $Ba(Fe_{0.963}Ni_{0.037})_2As_2$ ($T_c = 17$ K) disperses upwards. Using a simple mean-field approach with the assumption of $s^{\pm}$ order parameter, we show that the details of the dispersion, such as the resonance velocity, are determined by the normal state spin fluctuations.

The sample studied is a single crystal of $Ba(Fe_{1-x}Ni_x)_2As_2$, with $x = 0.037$ weighing 436 mg. Rather than using coaligned single crystals with a larger total mass, we chose to measure a single specimen of high crystallinity (mosaic width $<0.44°$) to minimize effects of sample mosaic on the **q** dependence of the spin fluctuations. Our preliminary neutron and x-ray scattering measurements show that the sample orders into an incommensurate AFM structure [11] below $T_N = 26$ K with a tetragonal-orthorhombic transition below $T_S = 29$ K. The superconducting transition temperature is $T_c = 17$ K. Additional details of crystal growth and characterization are described elsewhere [12]. The sample was mounted in a closed-cycle refrigerator for temperature dependent studies on the HB3 neutron spectrometer at the High Flux Isotope Reactor at Oak Ridge National Laboratory using pyrolitic

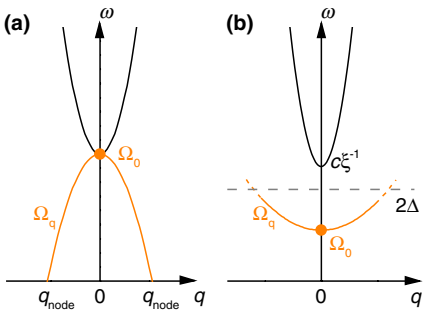


FIG. 1 (color online). (a) Spin fluctuations in the cuprates showing the hourglass shape of the spin excitations. The downward dispersing part [gray (orange) line] is the resonance mode for a *d*-wave gap and the upward part (black line) is the competing AFM spin fluctuations. (b) Spin fluctuations in our Ni-doped iron arsenide superconductor where both the resonance and competing AFM fluctuations disperse upwards.

 

graphite (0, 0, 2) reflections for both monochromator and analyzer and a configuration with $E_f = 14.7$ meV, 48′–60′–80′–120′ collimation and two pyrolitic graphite filters before the analyzer. We define $\mathbf{Q} = (H, K, L) = \frac{2\pi}{a}H\hat{\imath} + \frac{2\pi}{a}K\hat{\jmath} + \frac{2\pi}{c}L\hat{k}$, where the orthorhombic lattice constants, $a \approx b = 5.6$ Å and $c = 13$ Å were determined at $T = 15$ K. The crystal was aligned in the (1, 0, 1)-(0, 1, 0) scattering plane. Raw data were converted into the imaginary part of the magnetic susceptibility $\chi''(\mathbf{Q}, \omega)$ after subtracting estimates of the nonmagnetic background and correcting for the Bose population factor. In addition, we performed inelastic neutron scattering measurements on the Cold Neutron Chopper Spectrometer (CNCS) at the Spallation Neutron Source at Oak Ridge National Laboratory using an incident energy of 10 meV. Data were accumulated in the [$H$, $K$, 1] plane by rotating the crystal around a vertical (0, 1, 0) axis and performing a series of exposures.

Figure 2(a) shows the energy dependence of the imaginary part of the magnetic susceptibility $\chi''(\mathbf{Q}_{\mathrm{AFM}}, \omega)$ for $Ba(Fe_{0.963}Ni_{0.037})_2As_2$ in the normal state at $T = 20$ K and the superconducting state at $T = 4$ K, where $\mathbf{Q}_{\mathrm{AFM}} = (1, 0, 1)$ in orthorhombic coordinates. The neutron

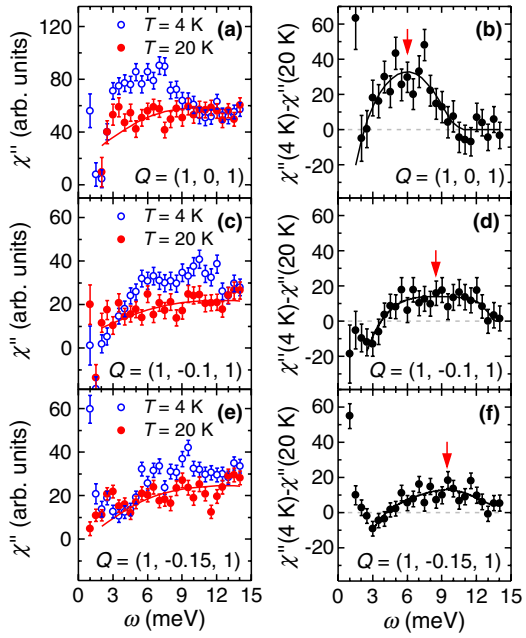


FIG. 2 (color online). The imaginary part of the magnetic susceptibility measured on HB3 at (a) $\mathbf{Q}_{\mathrm{AFM}} = (1, 0, 1)$, (c) $\mathbf{Q} = (1, -0.1, 1)$, and (e) $\mathbf{Q} = (1, -0.15, 1)$ in the normal state at $T = 20$ K (filled circles) and the superconducting state at $T = 4$ K (open circles). Solid red lines are model calculations of the normal state susceptibility assuming the NAFL spin fluctuations, as described in the text. The difference between superconducting and normal state susceptibilities is shown at (b) $\mathbf{Q}_{\mathrm{AFM}}$, (d) $\mathbf{Q} = (1, -0.1, 1)$, and (f) $\mathbf{Q} = (1, -0.15, 1)$. Black lines are guide to the eyes and arrows indicate the resonance peak obtained from Gaussian fit.

spin resonance peaks at an energy of $\Omega_0 \approx 6$ meV, as made clearer by the difference plot in Fig. 2(b) showing the resonance enhancement. At $\mathbf{Q}_{\mathrm{AFM}}$, the resonance extends up to approximately 10 meV, above which the susceptibilities of the normal and SC states are equivalent. Measurements of the energy spectrum at positions offset from $\mathbf{Q}_{\mathrm{AFM}}$ in the transverse direction [$\mathbf{Q} = (1, -0.1, 1)$ and $(1, -0.15, 1)$] show that the center of the resonance intensity shifts up to higher energy [Figs. 2(c)–2(f)]. In addition, we observe that the resonance spectral weight extends to at least 14 meV. Thus, despite the very broad line shapes, measurements of the susceptibility away from $\mathbf{Q}_{\mathrm{AFM}}$ show that the spectral weight of the resonance has moved to higher energy; i.e., *the resonance is dispersing upwards, unlike the cuprates*.

The observation of resonance dispersion is confirmed by a series of constant-energy $\mathbf{Q}$ scans in the normal and SC states in the vicinity of $\mathbf{Q}_{\mathrm{AFM}} = (1, 0, 1)$, focusing on the transverse direction $\mathbf{Q} = (1, K, 1)$ [$\mathbf{q} = (0, K, 0)$] as shown in Figs. 3(a) and 3(b). Here, the resonance is clearly identified by the enhanced susceptibility at $\mathbf{Q}_{\mathrm{AFM}}$ and $\omega \approx \Omega_0 = 6$ meV. As the energy is increased, the spectral weight progressively moves away from $\mathbf{Q}_{\mathrm{AFM}}$ and weakens. Plots of the difference between the susceptibility in the normal and superconducting states more clearly show that the resonance $\Omega_{\mathbf{q}}$ disperses upwards away from $\mathbf{Q}_{\mathrm{AFM}}$ [Fig. 3(b)]. In contrast, along the longitudinal ($H$, 0, $H$) direction in our scattering geometry, we find that only a weak resonance enhancement remains at $\mathbf{Q}_{\mathrm{AFM}}$ at 9 meV and no resonance enhancement is observed at 12 meV; i.e., there is surprisingly no indication of dispersion in the longitudinal direction [Figs. 3(e) and 3(f)]. This observation is consistent with early measurements of the resonance in both Ni (Ref. [13]) and Co-doped (Refs. [14–16]) $BaFe_2As_2$ that find a sharply defined resonance in the $H$ (orthorhombic **a**) direction. Thus, while the resonance dispersion is observed in the transverse direction, it is apparently too steep to observe a splitting in the longitudinal direction due to the limited instrumental resolution (we will return to this point below). As discussed below, the $\mathbf{Q}$-space anisotropy of the spin resonance in the SC state may be associated with the normal state spin fluctuations within the Fe layers that possess a twofold (elliptical) anisotropy [Fig. 3(e)] [17–20].

We now turn to a discussion of the spin dynamics in the normal and SC states, which leads to a straightforward interpretation of the resonance dispersion and its anisotropy. Despite the presence of weak AFM ordering, the normal state spin dynamics of the underdoped $BaFe_2As_2$ compounds at low energies can be understood using the model of nearly AFM Fermi liquids (NAFL) [17,21]. The imaginary part of the dynamical susceptibility, as measured by INS, can be written as in Ref. [21],

$$\chi_n''(\mathbf{q}, \omega) = \frac{\chi_0 \xi_{\mathbf{q}}^2 \Gamma_{\mathbf{q}} \omega}{\omega^2 + \Gamma_{\mathbf{q}}^2 [1 + \xi_{\mathbf{q}}^2 q^2]^2}, \qquad (1)$$

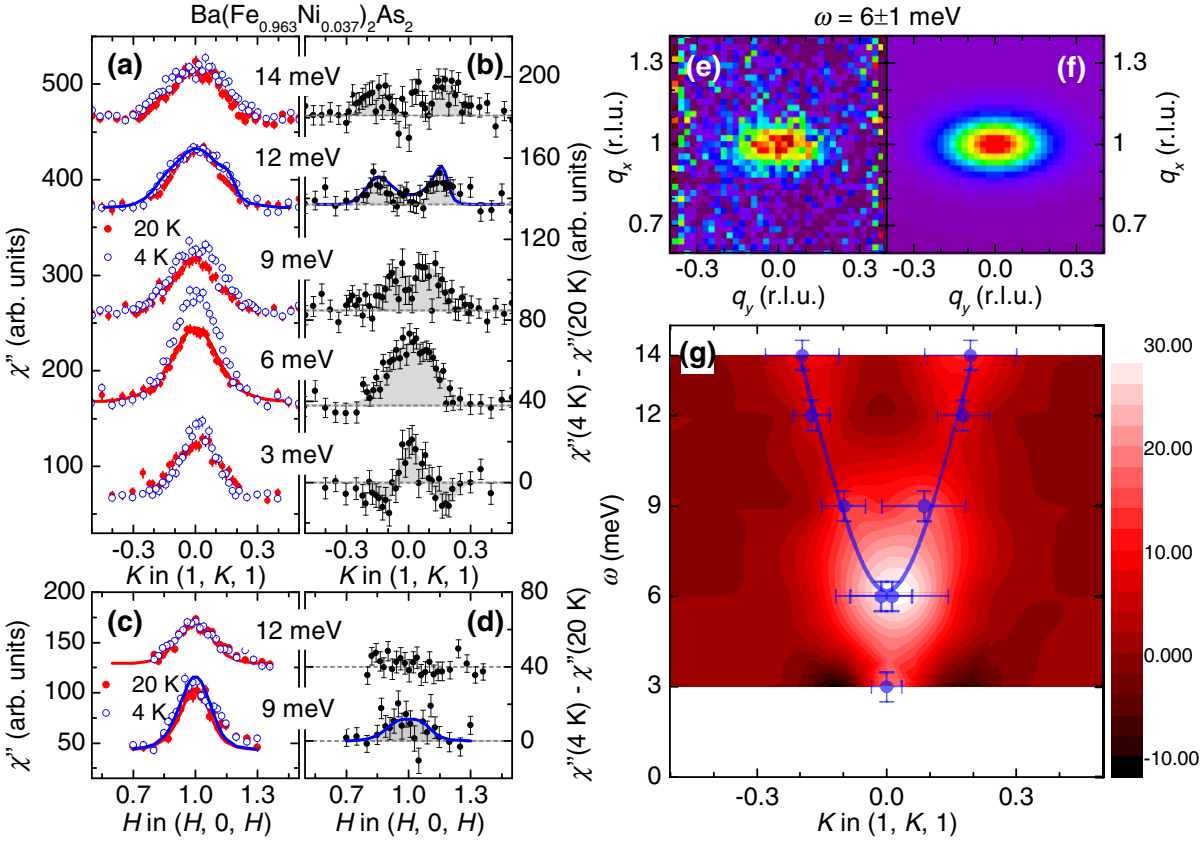


FIG. 3 (color online). (a) The imaginary part of the magnetic susceptibility measured on HB3 at various energy transfers along the [0, $K$, 0] direction transverse to $\mathbf{Q}_{\mathrm{AFM}} = (1, 0, 1)$ in the normal state at $T = 20$ K (filled circles) and the superconducting state at $T = 4$ K (open circles). (b) The difference of superconducting minus normal state susceptibilities from (a). (c) The susceptibilities along the [$H$, 0, $H$] direction longitudinal to $\mathbf{Q}_{\mathrm{AFM}}$ in the normal (filled circles) and superconducting states (open circles) and (d) the difference. Red and blue lines are model calculations of the normal state susceptibility and superconducting resonance, respectively, as described in the text. (e) CNCS measurements of the normal state spin fluctuations in the ($H$, $K$, 1) plane at $\omega = 6$ meV and $T = 25$ K. (f) Fit of the CNCS data to a model of NAFL, as described in the text. (g) Contour plot showing the difference of the magnetic susceptibilities in the superconducting and normal states measured on HB3 depicting the dispersion of the resonance in the transverse direction. Symbols correspond to fitted values of the resonance maxima and the line is a fit to the magnonlike dispersion given in Eq. (4). The vertical error bars indicate the energy resolution of HB3 and horizontal error bars indicate the FWHM of fits.

where $\xi_{\mathbf{q}}$ is the AFM correlation length, $\Gamma_{\mathbf{q}}$ is the relaxation width due to the decay of spin waves into electron-hole pairs (Landau damping), and the subscript $\mathbf{q}$ allows for anisotropy in these quantities.

The anisotropy of the normal state susceptibility has been studied in detail [19]. The twofold in-plane anisotropy of the magnetic correlation length is most important for the subsequent discussion,

$$\xi_{\mathbf{q}}^2 q^2 = \xi^2[q^2 + \eta(q_x^2 - q_y^2)], \tag{2}$$

and we assume in Eq. (1) that the damping $\Gamma_{\mathbf{q}} \approx \Gamma_0$ is isotropic and constant throughout the Brillouin zone. Since the resonance dispersion observed along the $L$ (**c**) direction in $A\mathrm{Fe}_2\mathrm{As}_2$ ($A$ = Ca, Sr, and Ba) based superconductors is weak, we assume $q_z$ gives a negligible effect. Typical fits to the normal state data in terms of the NAFL convolved with the instrumental resolution are shown in Figs. 2, 3(a), 3(c), and 3(f) with $\Gamma_0$ fixed to 10 meV [19]. We obtain the following parameters; $\xi = 9.5(4)$ Å and $\eta = 0.5(1)$ corresponding to different correlation lengths 11.8(7) Å and 6.5(3) Å in the $H$ (orthorhombic **a**) and $K$ (**b**) directions within the Fe layers, respectively.

The neutron spin resonance is reasonably well understood as an excitonic bound state in an itinerant antiferromagnet [1,2]. In this picture, fermions form singlet Cooper pairs and electron-hole (singlet-triplet) excitations appear with a threshold energy $|\Delta_{\mathbf{k}}| + |\Delta_{\mathbf{k}+\mathbf{Q}_{\mathrm{AFM}}}|$. These electron-hole excitations will form a bound state inside the SC gap (an exciton) as a consequence of interactions already present in the normal state. The spectral features of the bound state can be understood within a mean-field or random-phase approximation (RPA) approach to the interactions, as described below.

Following closely the arguments from Ref. [22], the RPA analysis of the susceptibility in the superconducting state leads to an equation for the dispersion of the resonance mode,

$$\Omega_{\mathbf{q}}^2 = \Delta_{\mathbf{q}}\Gamma_{\mathbf{q}}(1 + \xi_{\mathbf{q}}^2 q^2), \quad (3)$$

where $2\Delta_{\mathbf{q}} = |\Delta_{\mathbf{k}}| + |\Delta_{\mathbf{k}+\mathbf{Q}_{\mathrm{AFM}}+\mathbf{q}}|$ is the fermion gap at two points on the Fermi surface connected by $\mathbf{q} + \mathbf{Q}_{\mathrm{AFM}}$ and $\Omega_0 = \sqrt{\Delta_0\Gamma_0}$ is the resonance energy at $\mathbf{Q}_{\mathrm{AFM}}$ ($\mathbf{q} = 0$). Note that for a single-band model with a $d$-wave gap possessing nodes at $\mathbf{q}_{\mathrm{node}}$, $\Delta_0$ is a maximum and $\Delta_{\mathbf{q}_{\mathrm{node}}} \rightarrow 0$ at points on the Fermi surface, thereby forcing $\Omega_{\mathbf{q}_{\mathrm{node}}} \rightarrow 0$ and resulting in the downward dispersion shown in Fig. 1(a). The simple RPA model therefore captures the essential features resulting in the downward dispersion in the cuprates.

Although the $\mathbf{q}$ dependence of the resonance in Eq. (3) has several contributions (such as $\mathbf{q}$-dependent gap or damping effects), here we choose to apply the RPA approach for the iron arsenides under the assumption that the $\mathbf{q}$ dependence arises only from anisotropy in the normal state spin fluctuations. Assuming the proposed $s^{\pm}$ gap symmetry for our compound, $\Delta_{\mathbf{q}} = \Delta_0$ for all $\mathbf{q}$, and the equation above takes the form of a gapped magnon with upward dispersion,

$$\Omega_{\mathbf{q}} = \sqrt{\Omega_0^2 + c_{\mathrm{res},\mathbf{q}}^2 q^2}, \quad (4)$$

where $c_{\mathrm{res},\mathbf{q}}^2 = \Omega_0^2\xi_{\mathbf{q}}^2$ is the velocity of the resonance mode which becomes anisotropic itself due to the anisotropy in the normal state spin-spin correlation length. More detailed four-band RPA calculations (Ref. [23]) and two-orbital calculations of the susceptibility within the self-consistent fluctuation exchange approximation (Ref. [9]) arrive at similar conclusions regarding the upward resonance dispersion, at least at low doping concentrations. With increased electron doping, other multiband RPA calculations have predicted the development of an incommensurate normal state response [10,20,23]. In the superconducting state, these calculations predict that the resonance itself is also incommensurate and first disperses downwards to the incommensurate wave vector, and then upwards. Our observation highlighting the upward dispersing and commensurate response is, therefore, consistent with the multiband RPA approach for underdoped compositions. We note that an incommensurate resonance was reported for $Ba(Fe_{0.925}Ni_{0.075})_2As_2$ by Luo *et al.* [24] at a higher composition than reported here. This evolution towards an incommensurate response would be consistent with the general trend outlined above. However, the incommensurate splitting was only observed in the superconducting state (not in the normal state) and found to disperse upwards away from $\mathbf{Q}_{\mathrm{AFM}}$ rather than downwards.

We predict the anisotropic resonance velocities $\sqrt{\Omega_0^2\xi^2(1 \pm \eta)}$ in the Fe layers to be 85(5) and 50 (5) meV Å in the $H$ and $K$ directions, respectively, using values [$\xi = 9.5(4)$ Å and $\eta = 0.5(1)$] obtained from the normal state spin fluctuations. These predictions can be compared to fits made to the total susceptibility ($\chi'' = \chi_n'' + \chi_{\mathrm{res}}''$) after convolution with the instrumental resolution function, where $\chi_{\mathrm{res}}''$ is the resonance enhancement that obeys the dispersion relation in Eq. (4) and $\chi_n''$ is given by Eq. (1). Typical fits are shown as the solid blue line in Figs. 3(a) and 3(b). A contour plot of $\chi_{\mathrm{res}}''$ obtained from INS data along with fitted values of the peak positions is shown in Fig. 3(g), and we arrive at 63(2) meV Å for the observed resonance velocity in the $K$ direction, in good agreement with the simple analysis above.

The resonance velocity is to be contrasted with the velocity of the normal state AFM spin waves which are much steeper $c \approx 450$ meV Å $\gg c_{\mathrm{res}}$. Within the disordered AFM state model, dispersive features of the normal state AFM spin waves will appear only at much higher energies, $\omega > c\xi^{-1} \approx 60$ meV, as shown in Fig. 1(b). This disparity in the magnitude of the normal state and resonance velocities eliminates the possibility that resonance may be interpreted as damped AFM spin waves that sharpen up in the SC state (see Supplemental Material for more information [25]). We also note that limitations due to experimental resolution may prevent observation of the splitting in the longitudinal direction with the predicted velocity of 85(5) meV Å, as shown in Figs. 3(c) and 3(d).

In conclusion, we find that the dispersion of the neutron spin resonance in $Ba(Fe_{0.963}Ni_{0.037})_2As_2$ can be interpreted based on the assumption of extended $s$-wave superconductivity and the properties of the NAFL spin fluctuations in the normal state, most notably the anisotropic spin-spin correlation length. Such observations strongly support an excitonic picture for the spin resonance. Similar reasoning may also explain the weak resonance dispersion observed along the direction perpendicular to the layers ($L$ direction) in $AFe_2As_2$ based superconductors. For quasi-two-dimensional normal state spin fluctuations observed in optimally doped samples, the resonance will have no dispersion along $L$ (appear flat) due to the vanishing correlation length. However, underdoped samples with long-range AFM order, such as $Ba(Fe_{1-x}Co_x)_2As_2$ with $x = 0.04$ [16] and 0.047 [15,26], still possess weak interlayer spin correlations. Correspondingly, a finite, albeit small, $L$ dispersion is observed in these samples (with a velocity of ~6 meV Å). In a similar vein, doping will also affect both the interlayer and intralayer correlation length and, consequently, the resonance dispersion is expected to be composition dependent. This could explain recent observations of a large transverse resonance splitting in overdoped $Ba(Fe_{1-x}Ni_x)_2As_2$ [24].

The work at Ames Laboratory was supported by the U.S. Department of Energy, Office of Basic Energy Science, Division of Materials Sciences and Engineering under Contract No. DE-AC02-07CH11358. Work at Oak Ridge National Laboratory is supported by U.S. Department of Energy, Office of Basic Energy Sciences, Scientific User Facilities Division.

*mgkim@lbl.gov
†Corresponding author.
mcqueeney@ameslab.gov

[1] M. Eschrig, Adv. Phys. **55**, 47 (2006).
[2] T. A. Maier and D. J. Scalapino, Phys. Rev. B **78**, 020514 (2008).
[3] P. Bourges, Y. Sidis, H. F. Fong, L. P. Regnault, J. Bossy, A. Ivanov, and B. Keimer, Science **288**, 1234 (2000).
[4] S. Pailhès, Y. Sidis, P. Bourges, V. Hinkov, A. Ivanov, C. Ulrich, L. P. Regnault, and B. Keimer, Phys. Rev. Lett. **93**, 167001 (2004).
[5] I. I. Mazin, D. J. Singh, M. D. Johannes, and M. H. Du, Phys. Rev. Lett. **101**, 057003 (2008).
[6] G. Yu, Y. Li, E. M. Motoyama, and M. A. Greven, Nat. Phys. **5**, 873 (2009).
[7] D. S. Inosov, J. T. Park, A. Charnukha, Y. Li, A. V. Boris, B. Keimer, and V. Hinkov, Phys. Rev. B **83**, 214520 (2011).
[8] T. Das, R. S. Markiewicz, and A. Bansil, Phys. Rev. B **85**, 064510 (2012).
[9] J. Zhang, R. Sknepnek, and J. Schmalian, Phys. Rev. B **82**, 134527 (2010).
[10] T. A. Maier, P. J. Hirschfeld, and D. J. Scalapino, Phys. Rev. B **86**, 094514 (2012).
[11] M. G. Kim, J. Lamsal, T. W. Heitmann, G. S. Tucker, D. K. Pratt, S. N. Khan, Y. B. Lee, A. Alam, A. Thaler, N. Ni *et al.*, Phys. Rev. Lett. **109**, 167003 (2012).
[12] P. C. Canfield, S. L. Bud'ko, N. Ni, J. Q. Yan, and A. Kracher, Phys. Rev. B **80**, 060501 (2009).
[13] S. Chi, A. Schneidewind, J. Zhao, L. W. Harriger, L. Li, Y. Luo, G. Cao, Z. Xu, M. Loewenhaupt, J. Hu *et al.*, Phys. Rev. Lett. **102**, 107006 (2009).
[14] M. D. Lumsden, A. D. Christianson, D. Parshall, M. B. Stone, S. E. Nagler, G. J. MacDougall, H. A. Mook, K. Lokshin, T. Egami, D. L. Abernathy *et al.*, Phys. Rev. Lett. **102**, 107005 (2009).
[15] D. K. Pratt, W. Tian, A. Kreyssig, J. L. Zarestky, S. Nandi, N. Ni, S. L. Bud'ko, P. C. Canfield, A. I. Goldman, and R. J. McQueeney, Phys. Rev. Lett. **103**, 087001 (2009).
[16] A. D. Christianson, M. D. Lumsden, S. E. Nagler, G. J. MacDougall, M. A. McGuire, A. S. Sefat, R. Jin, B. C. Sales, and D. Mandrus, Phys. Rev. Lett. **103**, 087002 (2009).
[17] S. O. Diallo, D. K. Pratt, R. M. Fernandes, W. Tian, J. L. Zarestky, M. Lumsden, T. G. Perring, C. L. Broholm, N. Ni, S. L. Bud'ko *et al.*, Phys. Rev. B **81**, 214407 (2010).
[18] H.-F. Li, C. Broholm, D. Vaknin, R. M. Fernandes, D. L. Abernathy, M. B. Stone, D. K. Pratt, W. Tian, Y. Qiu, N. Ni *et al.*, Phys. Rev. B **82**, 140503 (2010).
[19] G. S. Tucker, R. M. Fernandes, H.-F. Li, V. Thampy, N. Ni, D. L. Abernathy, S. L. Bud'ko, P. C. Canfield, D. Vaknin, J. Schmalian *et al.*, Phys. Rev. B **86**, 024505 (2012).
[20] J. T. Park, D. S. Inosov, A. Yaresko, S. Graser, D. L. Sun, P. Bourges, Y. Sidis, Y. Li, J.-H. Kim, D. Haug *et al.*, Phys. Rev. B **82**, 134503 (2010).
[21] D. S. Inosov, J. T. Park, P. Bourges, D. L. Sun, Y. Sidis, A. Schneidewind, K. Hradil, D. Haug, C. T. Lin, B. Keimer *et al.*, Nat. Phys. **6**, 178 (2009).
[22] A. V. Chubukov, B. Jankó, and O. Tchernyshyov, Phys. Rev. B **63**, 180507 (2001).
[23] S. Maiti, J. Knolle, I. Eremin, and A. V. Chubukov, Phys. Rev. B **84**, 144524 (2011).
[24] H. Luo, Z. Yamani, Y. Chen, X. Lu, M. Wang, S. Li, T. A. Maier, S. Danilkin, D. T. Adroja, and P. Dai, Phys. Rev. B **86**, 024508 (2012).
[25] See Supplemental Material at http://link.aps.org/supplemental/10.1103/PhysRevLett.110.177002 for the derivation of the dynamical magnetic susceptibility of itinerant antiferromagnet in the normal and superconducting states.
[26] D. K. Pratt, A. Kreyssig, S. Nandi, N. Ni, A. Thaler, M. D. Lumsden, W. Tian, J. L. Zarestky, S. L. Bud'ko, P. C. Canfield *et al.*, Phys. Rev. B **81**, 140510 (2010).